SUPPORTING INFORMATION

Pb^{2+} as modulator of protein-membrane interactions

Krystal A. Morales,[†] Mauricio Lasagna,[†] Alexey V. Gribenko,[§,≠] Youngdae Yoon,[#] Gregory D. Reinhart,[†] James C. Lee,[§] Wonhwa Cho,[#] Pingwei Li,[†] and Tatyana I. Igumenova[†,]*

[†]Department of Biochemistry and Biophysics, Texas A&M University, College Station, TX 77843;

[#]Department of Chemistry, University of Illinois at Chicago, Chicago, IL 60607;

[§]Department of Biochemistry and Molecular Biology, The University of Texas Medical Branch at Galveston, Galveston, TX 77555.

[≠]Current address: Pfizer, Pearl River, NY 10965.

*Corresponding author: Tatyana I. Igumenova, phone: (979) 845 6312, fax: (979) 845 4946, e-mail: tigumenova@tamu.edu.

1. Over-expression and purification of C2α

C2α over-expression was carried out in *E. coli* BL21(DE3) cells. Cell cultures were grown to an OD_{600} of 0.6 and induced with 0.5 mM IPTG for 4 hours at 37 °C for all natural abundance preparations. Isotopically enriched protein was over-expressed according to the method of Marley et al.,[1] with overnight induction at 15 °C. The M9 minimal media was supplemented with 1 g/L of $^{15}NH_4Cl$ and 3 g/L of [^{13}C-6]-D-glucose (or natural abundance D-glucose) as sole nitrogen and carbon sources, respectively. Fractionally deuterated protein sample was produced using M9 minimal media containing 75% $^{2}H_2O$, 3 g/L of [^{13}C-6]-D-glucose, and 1 g/L of $^{15}NH_4Cl$.

The histidine-tagged SUMO-C2α fusion protein was purified using a HisTrap™ HP Ni affinity column (GE Healthcare Life Sciences). The fractions containing fusion protein were desalted on a HiPrep 26/10 column (GE Healthcare Life Sciences). Isolated C2α domain was obtained by cleaving the fusion protein for 30 minutes with histidine-tagged SUMO protease at room temperature, followed by another Ni affinity purification step to remove the histidine-tagged SUMO and SUMO protease. The final purification step was cation-exchange chromatography on a Source 15S column (GE Healthcare Life Sciences), carried out in 10 mM 2-(N-morpholino)ethanesulfonic acid (MES) buffer at pH = 6.0, 0.1 mM EDTA, and a linear concentration gradient of KCl. The purity of C2α was evaluated using SDS-PAGE. The molecular weight was verified by MALDI-TOF mass spectrometry.

2. Data collection and structure determination of apo- and Pb^{2+}-bound C2α

All diffraction data were collected using a Rigaku RAXIS IV^{++} image plate detector mounted on a Rigaku Micromax-007HF generator. The data were processed with the HKL2000 package.[2]

The apo-C2α domain crystallized in space group $P3_221$ with the following cell parameters: a=b= 58.00 Å, c=90.46 Å, and γ=120°. The crystallographic asymmetric unit (ASU) contains one C2α molecule. The Pb^{2+}-bound C2α also crystallized in space group $P3_221$ with slightly different unit cell dimensions: a=b=58.29 Å, c=87.98 Å. The structure of the Pb^{2+}-bound C2α was determined by

molecular replacement using MOLREP in the CCP4 suite. The Ca^{2+}-bound C2α structure after the deletion of the Ca^{2+} ions (PDB code: 1DSY)[3] was used as a search model. The electron density map for the Pb^{2+} ions was apparent in the $2F_o$-F_c difference map (**Figure S1A**). Only two strong peaks corresponding to the lead ions were observed in the anomalous difference map (**Figure S1B)**, indicating that there was no nonspecific binding. The structural models were rebuilt using O and refined by several rounds of positional and B-factor refinement using CNS. Structure of the apo-C2α was refined using the high- resolution lead-bound C2 domain as a starting model. The structure was rebuilt with O and refined with CNS. The coordinates were submitted to the Protein Data Bank (http://www.pdb.org/) and were assigned the ID codes of 3RDJ and 3RDL for the apo- and Pb^{2+}-bound structures, respectively.

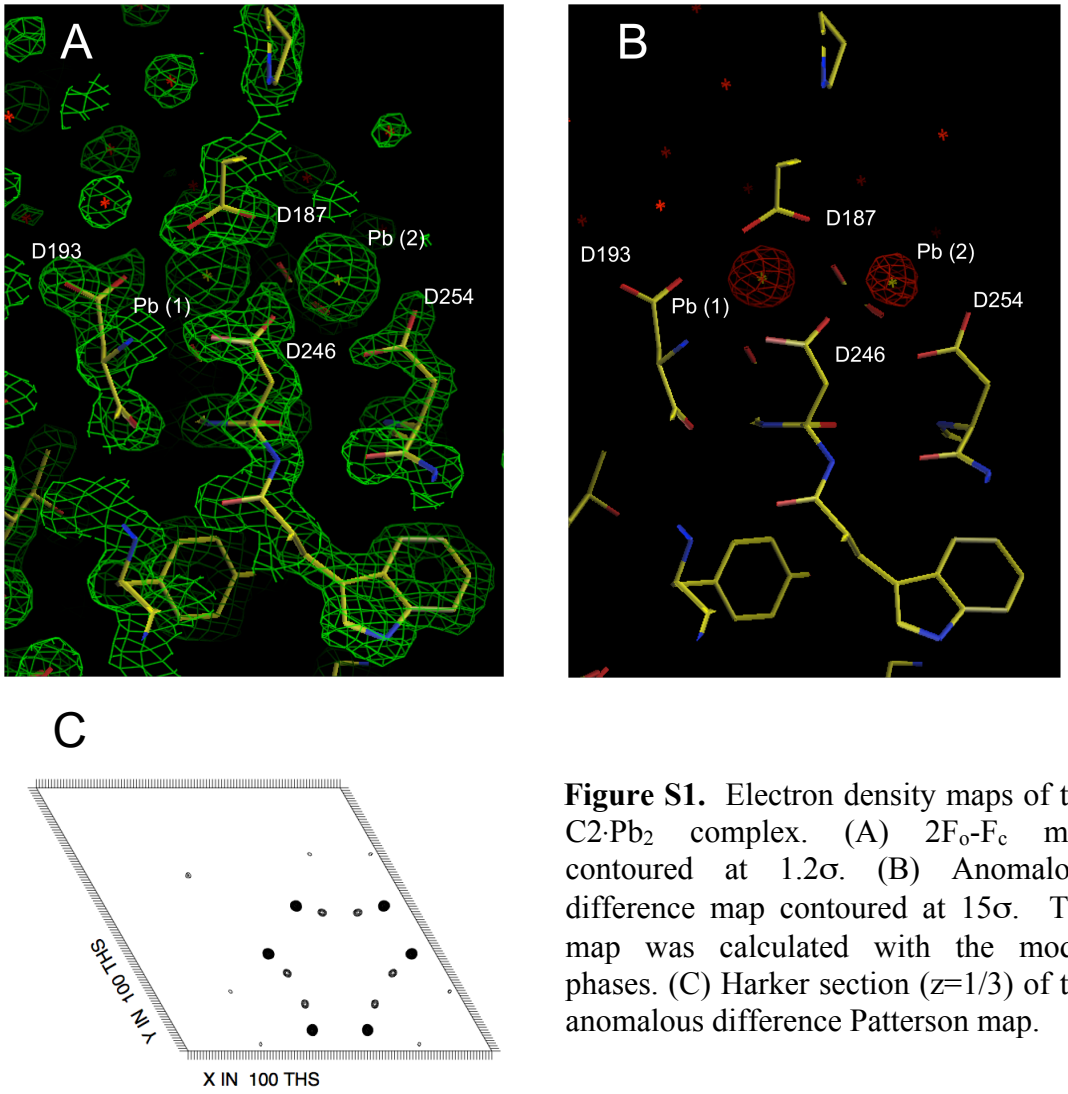

Figure S1. Electron density maps of the C2·Pb_2 complex. (A) $2F_o$-F_c map contoured at 1.2σ. (B) Anomalous difference map contoured at 15σ. The map was calculated with the model phases. (C) Harker section (z=1/3) of the anomalous difference Patterson map.

Table S1. Crystallographic data collection and refinement statistics.

Diffraction Data	**Apo C2α**	**Pb^{2+}-bound C2α**
Wavelength (Å)	1.542	1.542
Space group	$P3_221$	$P3_221$
Unit cell	a=b=58.00 Å, c=90.46 Å	a=b=58.29 Å, c=87.98 Å
Resolution (Å)	50.0-1.90 (1.97-1.90)[a]	50.0-1.50 (1.55-1.50)[a]
Unique reflections	14383	27889
Redundancy	6.3 (6.2)	6.5 (4.0)
Completeness	99.8% (99.7%)	98.3 (93.2)
<I/σI>	47.5 (5.2)	60.4 (5.6)
R_{sym}(%)	5.3 (45.4)	7.4 (32.3)
Refinement		
Resolution (Å)	50.0-1.90	50.0-1.50
Reflections (F>0) (total/test set)	14022/1438	51491/5041
Protein atoms	1129	1129
Pb (II) ions	0	2
Sulfate ions	0	4
Solvent atoms	107	205
R_{cryst}/R_{free}	22.5%/24.5%	20.4%/21.9%
RMSD, bond length	0.010 Å	0.011 Å
RMSD, bond angle	1.67°	1.67°

[a]Values in the parentheses are for the highest-resolution shell; 10% of reflections are used in the test set for the R_{free} calculation.

3. NMR-detected binding of Ca^{2+} to apo C2α

NMR-detected Ca^{2+} binding experiments were carried out as described in the Experimental Section. It is evident from the NMR spectra that the metal-binding sites of C2α have comparable affinities to Ca^{2+} ions. The presence of three species, C2α·Ca(1), C2α·Ca(2) and C2α·$(Ca)_2$, each having its own chemical shift, precludes the use of an analytical function to describe the binding process. In addition, all Ca^{2+} binding curves show a lag period, indicating some degree of positive cooperativity. To estimate the binding affinity, we fit the curves individually with the Hill equation. The range of apparent K_d values is 250-530 μM, with the median of 350 μM. This range reflects the differential response of C2α residues to Ca^{2+} binding and the approximation, under which the concentration of free ligand is considered to be approximately equal to the total concentration of the ligand. Correction for the free ligand concentration, implemented as described for the C2 domain of rabphilin-3A,[4] gives a K_d range of 150-480 μM with the median of 270 μM. Several representative Ca^{2+} binding curves are shown below for the residues that belong to Ca^{2+}-binding loop regions CBL1, CBL2, and CBL3.

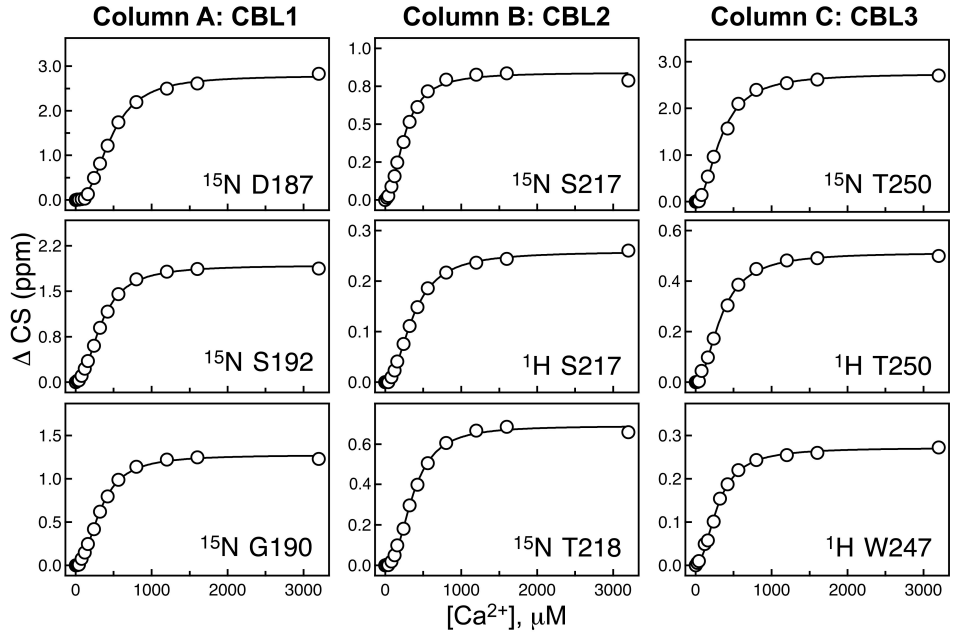

Figure S2. Representative Ca^{2+} binding curves for residues that belong to Ca^{2+}-binding loops (CBLs) 1, 2, and 3. The absolute change in chemical shift is plotted as a function of the total Ca^{2+} concentration. The fits were generated using the Hill equation. C2α concentration is 160 μM.

4. Estimation of the Ca^{2+} binding affinity to the preformed C2α·Pb complex

We interpreted the results of Ca^{2+} binding to the *preformed* C2α·Pb complex using a set of the following equilibria:

$$C2\alpha + Pb^{2+} \overset{1}{\rightleftharpoons} C2\alpha\cdot Pb$$
$$C2\alpha\cdot Pb + Ca^{2+} \overset{2}{\rightleftharpoons} C2\alpha\cdot Pb\cdot Ca$$
$$C2\alpha\cdot Pb\cdot Ca + Ca^{2+} \overset{3}{\rightleftharpoons} C2\alpha\cdot Ca_2 + Pb^{2+}$$
$$C2\alpha\cdot Ca_2 + Ca^{2+} \overset{4}{\rightleftharpoons} C2\alpha\cdot Ca_3$$

The objective is to estimate the dissociation constant K_d of the C2α·Pb·Ca complex in Step 2. This constant can be determined from the NMR data by fitting the dependence of the chemical shift on the total concentration of Ca^{2+} using Eq. (1) from the Experimental Section. However, Ca^{2+} is also consumed in Steps 3 and 4 to form the Ca^{2+}-bound protein species. Hence, we wanted to estimate the extent to which the total Ca^{2+} concentration has to be modified to reflect the depletion of the Ca^{2+} pool. We selected three Ca^{2+} concentration points for the analysis: 3.2, 8.0, and 20 mM. The corresponding populations of the Ca-bound protein species (P_{Ca}) are 0.365, 0.457, and 0.615. The calcium mass balance equations are:

$$\frac{[Ca^{2+}]_T}{P_0} = \frac{[Ca^{2+}]_F}{P_0} + P_{PbCa} + 2P_{Ca2} + 3P_{Ca3} = \frac{[Ca^{2+}]_F}{P_0} + P_{PbCa} + 2P_{Ca} + P_{Ca3} \qquad \text{(Eq. S1)}$$

$$\text{where } P_{Ca} = P_{Ca2} + P_{Ca3}. \qquad \text{(Eq. S2)}$$

$[Ca^{2+}]_T$ is the total concentration of Ca^{2+}; $[Ca^{2+}]_F$ is the concentration of free Ca^{2+}; P_0=160 μM is the total concentration of C2α; P_{PbCa}, P_{Ca2}, and P_{Ca3} are the fractional populations of the C2α·Pb·Ca, $C2\alpha\cdot Ca_2$, and $C2\alpha\cdot Ca_3$ species, respectively. P_{Ca} values were determined from the Ca^{2+} titration of the *preformed* C2α·Pb complex. For the purpose of estimating the K_d, we assume that $C2\alpha\cdot Ca_2$ species fully convert into $C2\alpha\cdot Ca_3$ over the $[Ca^{2+}]_T$ range of 3.2-20 mM. Then, P_{Ca3} is 0, ~0.23, and ~0.61 for the three selected Ca^{2+} concentration points. Using Equations S1 and S2, we calculate $[Ca^{2+}]_F$ + [C2α·Pb·Ca] to be 3.0, 7.7, and 19.6 mM. These numbers are within 7% of the corresponding $[Ca^{2+}]_T$ values. This means that total Ca^{2+} concentrations can be used instead of $[Ca^{2+}]_F$ to construct the binding

curves for Step 2. Several binding curves with fits generated using Eq. (1) are shown in **Figure S3**. The dissociation constant was found to be 13±1 mM. Fitting the curves using a P_0 value that has been adjusted for the redistribution of Ca-only and Pb-containing species produced the same value of K_d within experimental error.

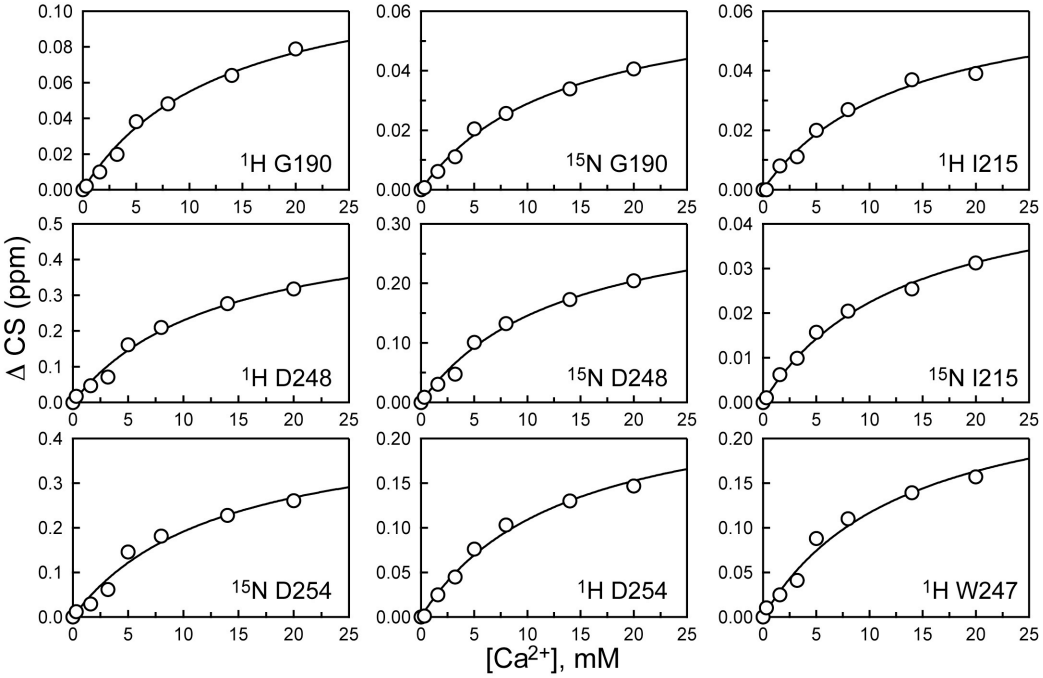

Figure S3. Ca^{2+} binding curves for residues of the preformed C2α·Pb complex. The absolute change in chemical shift is plotted as a function of the total Ca^{2+} concentration. The fits were generated using Eq. (1) of the Experimental Section.

5. Cryoelectron microscopy of the LUV suspensions in the presence of divalent metal ions

To verify the integrity of the LUVs in the presence of Pb^{2+}, we collected cryoelectron microscopy (cryoEM) images of the vesicle suspensions. For comparison, we also acquired images of LUVs in the presence of Ca^{2+}. The total concentrations of metal ions and lipid were 1 mM and 1.5 mM, respectively. For metal ions, 1 mM is the maximum concentration that was used in our ultracentrifugation binding assays. The concentration of the PtdSer lipid component adjusted for the leaflet distribution was 248 μM.

5 μl of the LUV suspension pre-incubated with the respective metal ion was applied onto a carbon-coated copper grid. The grids were rendered hydrophilic by glow discharging. The grids were then

plunge-frozen in liquid ethane using an FEI Vitrobot. Samples were observed on a Tecnai G2 F20 FE-TEM instrument equipped with a GATAN Tridiem imaging filter. The acceleration voltage was 200 kV.

The cryoEM images are shown in **Figure S4**. Compared to Ca^{2+}, high concentrations of Pb^{2+} promote vesicle aggregation. However, the LUVs are intact and show a rather uniform size distribution. Based on these data, we concluded that Pb^{2+}-induced dissociation of C2α from membranes is not due to the loss of structural integrity of LUVs.

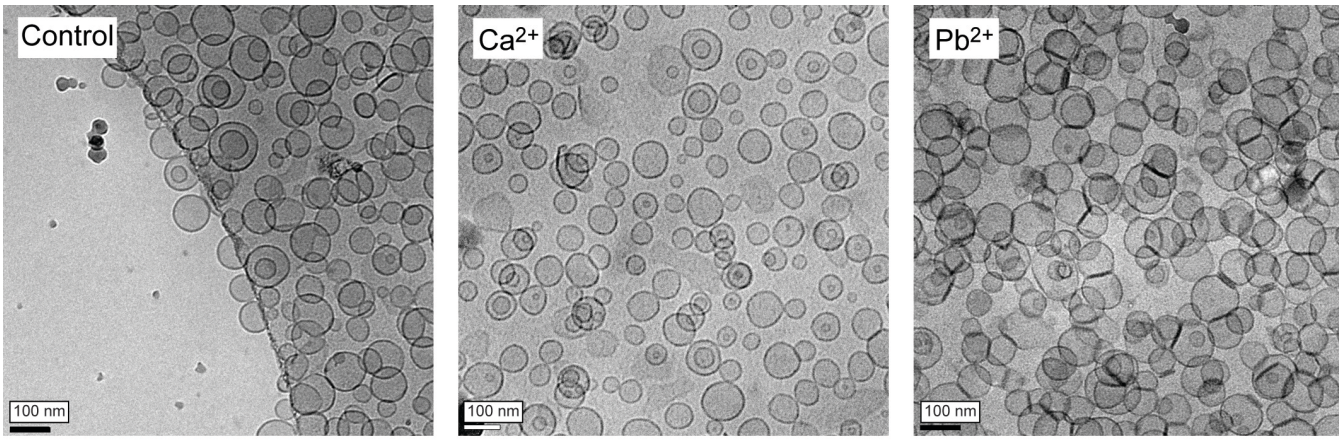

Figure S4. CryoEM images of LUVs (1.5 mM total lipid, POPS/POPC molar fractions of 33:67) in the absence of divalent metal ions (A) and in the presence of Ca^{2+} (B) and Pb^{2+} (C).

6. Association of Pb^{2+} with PtdSer-containing membranes quantified by inductively coupled plasma (ICP) measurements

To determine if Pb^{2+} can associate with lipid membranes, we carried out an ultracentrifugation binding experiment as described in the Experimental Section, but without the protein. The concentrations of Pb^{2+} in the supernatant ($[Pb^{2+}]_{free}$) and pellet ($[Pb^{2+}]_{bound}$) fractions were determined using ICP measurements. In brief, samples were digested with Fisher Optima nitric acid, hydrogen peroxide, and hydrochloric acid and diluted to the desired volume with 18.2 MΩ MilliQ water. The measurements were carried on a Perkin Elmer DRC 2 inductively coupled plasma mass spectrometer. The samples were run in the "standard mode" using external calibration, with Bi-209 as the internal standard.

The total Pb^{2+} concentration varied from 0 to 1 mM, and the total lipid concentration was 1.5 mM. The total concentration of the PtdSer component, adjusted for the distribution between the inner and outer leaflets of the bilayer was 248 μM. The fractional population of Pb^{2+}-bound PtdSer, θ, was calculated as: $\theta = [\text{PtdSer}]_{\text{bound}} / [\text{PtdSer}]_{\text{total}}$. The data were fit using the following equation for single-site binding:

$$\theta = \frac{[Pb^{2+}]_{\text{free}}}{K_d + [Pb^{2+}]_{\text{free}}}$$

where K_d is the dissociation constant for the Pb^{2+}-PtdSer complex. The experimental data and the fit are shown in **Figure S5**. The K_d was determined to be 119±12 μM.

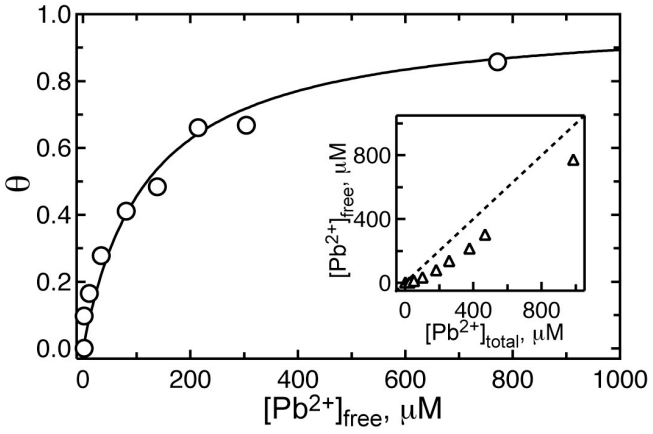

Figure S5. Pb^{2+} binding to 67% POPC:33% POPS LUVs quantified by ICP analysis. θ is the fractional population of Pb^{2+}-bound PtdSer. The inset shows the relationship between the total and free Pb^{2+}.

7. Coordination preferences of protein-bound oxygen-coordinated Pb^{2+}

The 23 protein structures, in which Pb^{2+} has at least one oxygen ligand have the following PDB identifiers: 1AFV, 1E9N, 1FJR, 1HD7, 1HQJ, 1KA4, 1N0Y, 1NA0, 1QNV, 1QR7, 1SN8, 1SYY, 1XXA, 1ZHW, 1ZHY, 2ANI, 2CH7, 2EX3, 2FP1, 2G0A, 2O3C, 2V01, and 2XAL. The structure of the zebra fish apurinic/apyrimidinic endonuclease (PDB ID 2O3C) was excluded from the analysis because of the partial occupancy of Pb sites. We further refined our criteria by requiring that (i) all ligands are oxygens and (ii) Pb^{2+} replaces a metal cofactor rather than being non-specifically adsorbed on the protein surface. The 14 Pb^{2+} sites that met these criteria and their corresponding PDB identifiers are listed in **Table S2**. The distribution of Pb-O bond lengths for these 14 sites is shown in **Figure S6**.

Table S2. Pb^{2+} sites selected for the Pb-O distance analysis.

PDB ID	Total number of Pb sites	Retained unique all-oxygen sites	Pb serial numbers
1E9N	4	2	4339, 4342
1HD7	1	1	2072
1N0Y	14	4	1315, 1317, 1328, 1330
2G0A	2	1	4655
2XAL	4	2	6758, 6759
2V01	8	4	1117, 1118, 1119, 1120
Total: 14 sites			

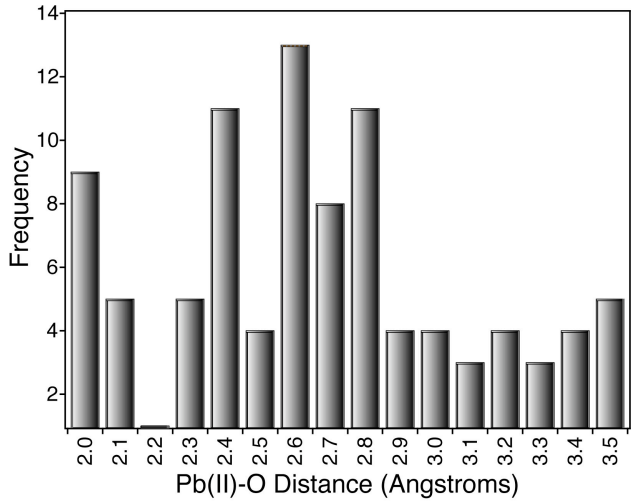

Figure S6. Histogram of the Pb-O distances measured for 14 all-oxygen Pb^{2+} sites.

REFERENCES

(1) Marley, J.; Lu, M.; Bracken, C. *J. Biomol. NMR* **2001**, *20*, 71.

(2) Otwinowski, Z.; Minor, W. *Macromolecular Crystallography, Pt. A* **1997**, *276*, 307.

(3) Verdaguer, N.; Corbalan-Garcia, S.; Ochoa, W. F.; Fita, I.; Gomez-Fernandez, J. C. *EMBO J.* **1999**, *18*, 6329.

(4) Montaville, P.; Coudevylle, N.; Radhakrishnan, A.; Leonov, A.; Zweckstetter, M.; Becker, S. *Protein Sci.* **2008**, *17*, 1025.